CLM-P789

CLM-P789

UKAEA

Preprint

THE STABILITY AND ACCURACY OF EPIC ALGORITHMS

J. W. EASTWOOD

CULHAM LABORATORY
Abingdon, Oxfordshire
1987

CLM-P789

THE STABILITY AND ACCURACY OF EPIC ALGORITHMS

James W.Eastwood
UKAEA, Culham Laboratory,
Abingdon, Oxon, OX14 3DB, U.K.
(Euratom/UKAEA Fusion Association)

July, 1986

Abstract

In the absence of particle discretisation effects (quadrature errors) EPIC algorithms give accurate and unconditionally stable schemes for integrating kinematic fluid and mhd equations. If particle discretisation is introduced as a consistently applied trapezium rule quadrature, then unconditional stability is retained. However, it is shown that not all quadratures lead to stable schemes.

General results on linear stability are given. An analysis of dispersive and dissipative effects of finite particle number is presented, and the efficacy of the algorithms is illustrated by kinematic and dynamic test problems. The kinematic test with discrete particles showed unexpected stability and accuracy for large Courant numbers.

(Submitted for publication in Computer Physics Communications)

1. Introduction.

EPIC algorithms [1,2,3] arise from optimal particle-mesh methods originally developed for collisionless phase fluids. In high dimensional phase space and shocked fluid flows, the Lagrangian sample points (particles) are the natural principal information carriers. However, in low (≤ 3) dimensional smooth flows, the mesh can become a more cost effective alternative. Here, we concentrate on the latter case, where particles are treated either as conceptual devices or as quadrature points in evaluating difficult integrals. Which alternative is appropriate depends on the choice of integration method.

In this paper, we show that Galerkin EPIC schemes remain stable if uniform quadrature is applied consistently to the projection equation. If the quadrature points are shifted with respect to the mesh, then unstable schemes can be found. Unstable schemes may be interpreted as applying too much 'antidiffusion' through the mass matrix. The discussions presented are given for the one dimensional case. Generalisation to higher dimensions is straightforward.

2. Zero quadrature errors.

Let

$$\frac{\partial f}{\partial t} + v \frac{\partial f}{\partial x} = 0 \qquad (1)$$

The Galerkin EPIC scheme advances the discrete approximation $f \simeq W_p(x) f_p$ at each timestep, Δt, according to the prescription

$$\left[\int W_q(x) W_p(x) dx\right] f_p^{t+\Delta t} = \left[\int W_q(x) W_p(x_o) dx\right] f_p^t \qquad (2)$$

where sums are implied over repeated indices and we treat x as a Lagrangian coordinate;

$$x = x(x_o, t) = x_o + \xi.$$

We restrict our attention to uniform unit node spacing and uniform advection. The basis functions W then have the displacement invariance property

$$W_p(x) = W_o(x - p) \equiv W(x - p) \tag{3}$$

and Eq.(2) reduces to

$$I(q - p,0)\ f_p^{t+\Delta t} = I(q - p,\xi)\ f_p^t \tag{4}$$

where the sum over p is implied and

$$I(q - p,\xi) = \int W(x)\ W(x - (p - q + \xi))\ dx \tag{5}$$

setting $f_p \propto - e^{i\omega t}$ and Fourier transforming Eq.(4) gives the dispersion relation

$$e^{i\omega\Delta t} = \frac{\tilde{I}(k,\xi)}{\tilde{I}(k,o)} \tag{6}$$

and the linear stability condition

$$\left|\frac{\tilde{I}(k,\xi)}{\tilde{I}(k,0)}\right| \leqslant 1 \tag{7}$$

If we let

$$H(X) = \int_{-\infty}^{+\infty} W(x)\ W(x - X)\ dx \tag{8}$$

then its Fourier transform is

$$\tilde{H}(k) = \left|\tilde{W}(k)\right|^2 \tag{9}$$

The set of nodal values $\{I(p,\xi)\}$ can be represented by the generalised function

$$I^+(x) = \text{ш}(x - \xi)H(x) \supset \tilde{I}(k,\xi) = \text{ш}\left(\frac{k}{2\pi}\right)\ e^{-ik\xi}{}_*\ \tilde{H}(k) \tag{10}$$

where the transform, ш and convolution (*) definitions follow those used

in reference [4]. Evaluating the convolution on the r.h.s. of Eq.(6) yields

$$\left|\frac{\tilde{I}(k,\xi)}{\tilde{I}(k,0)}\right| \equiv \left|\frac{\sum_{n=-\infty}^{\infty} |\tilde{W}(k_n)|^2 e^{i2\pi n\xi}}{\sum_{n=-\infty}^{\infty} |\tilde{W}(k_n)|^2}\right| \leq 1 \qquad (11)$$

thus demonstrating unconditional stability for all choices of W. k_n is the aliased wavenumber, $k_n = k - 2\pi n$.

The integrals appearing in Eq.(2) are only easy to evaluate in one dimension. However, if a uniform mesh is employed in two or more dimensions, then fractional timestepping can be employed. A displacement $\underset{\sim}{\xi} = (\xi_x, \xi_y)$ may be represented by a sequence $(\xi_x, 0)$, $(0, \xi_y)$ or to second order by a similar time symmetrised sequence of x, y, y, x displacements, etc. A general element connectivity is best tackled using quadrature.

3. Uniform Quadrature.

The simplest example of quadrature, which is readily generalised to higher dimensions, is obtained when integrals in Eq.(2) are replaced by sums (trapezoidal rule):-

$$\left[\sum_i W_q(x_i) W_p(x_i)\,\delta\right] f_p^{t+\Delta t} = \left[\sum_i W_q(x_i) W_p(x_{oi})\,\delta\right] f_p^t \qquad (12)$$

There are $M = 1/\delta$ uniformly spaced points in each element ("particles per cell") where positions $x_i = (i + \varepsilon)\delta$ and offset ε $\varepsilon[o,1]$.

Following the procedure used for the integral case, we may write Eq.(12) as

$$S(q - p, 0) f_p^{t+\Delta t} = S(q, p, \xi) f_p^t \qquad (13)$$

yielding the stability criterion

$$\left|\frac{\tilde{S}(k,\xi)}{\tilde{S}(k,0)}\right| \leq 1 \qquad (14)$$

where $S \supset \tilde{S}$.

Theorem: The projection scheme, Eq.(12) is stable for piecewise linear functions $W_p(x)$ if $\varepsilon = 0$ is used in evaluating the mass matrix appearing on the l.h.s.

Proof:

Let

$$H(X) = \int_{-\infty}^{\infty} \text{III}\,(Mx - \varepsilon)\, W(x)\, W(x-X)\, dx$$

$$\supset \tilde{H}(k) = \tilde{W}(k) \sum_{m=-\infty}^{\infty} \tilde{W}(k - 2\pi mM) e^{-i2\pi m\varepsilon} \qquad (15)$$

where III and transform definition follow the notation of [4]. Then we may represent the set $\{S(p,\xi)\}$ by the generalised function

$$S^{+}(x) = \text{III}(x - \xi)\, H(x)$$

$$\supset \tilde{S}(k,\xi) = \sum_{n=-\infty}^{\infty} \tilde{H}(k - 2\pi n) e^{-i2\pi n\xi} \qquad (16)$$

For piecewise linear functions, $W(x)$ (= if $|x| \leq 1$ then $1 - |x|$ else 0) $\supset$ $\tilde{W}(k) = \sin^2(k/2\pi)$, so $\tilde{H} \geq 0$ for all k, and therefore

$$\left|\frac{\tilde{S}(k,\xi)}{\tilde{S}(k,0)}\right| = \left|\frac{\sum_n \tilde{H}(k-2\pi n)\, e^{-i2\pi n\xi}}{\sum_n \tilde{H}(k-2\pi n)}\right| \leq 1 \qquad \text{q.e.d.}$$

Corollary:- If the mass matrix on the l.h.s of (12) is lumped, then scheme remains stable.

Proof

Lumping the l.h.s. of Eq.(12) reduces it to $f_q^{t+\Delta t}$ and the stability condition to $|\tilde{S}(k,\xi)| \leq 1$. But

$$\tilde{S}(k,0) = \frac{2+\delta^2}{3} + \left(\frac{1-\delta^2}{3}\right)\cos k \leq 1$$

$$\therefore \left|\tilde{S}(k,\xi)\right| \leq \tilde{S}(k,0) \leq 1 \qquad \text{q.e.d.}$$

If lumping is used, or if $\varepsilon \neq 0$ on the r.h.s. of Eq.(12), then we have schemes which will diffuse f, even in the limit $\Delta t \to 0$ (c.f. the Lax finite difference scheme [5]). For example, setting $\xi = 0$, $\varepsilon = 0$ on the l.h.s. and $\varepsilon = 1/2$ on the r.h.s. of Eq.(12) gives

$$f^+_p + \left(\frac{1-\delta^2}{6}\right)\left(f^+_{p+1} - 2f^+_p + f^+_{p-1}\right) = f_p + \left(\frac{2+\delta^2}{12}\right)\left(f_{p+1} - 2f_p + f_{p-1}\right)$$

showing quadrature errors introduce an effective diffusion coefficient $\propto \delta^2/\Delta t$. Whilst this may be of value in shocked flows, it is undesirable in low dissipation smooth flows. The symmetry of this example shows that if $\varepsilon \neq 0$ on the l.h.s. of Eq.(12), then unstable schemes can result. In particular, $\varepsilon = 1/2$ on the l.h.s. and $\varepsilon = 0$ on the r.h.s. gives a <u>negative</u> diffusion coefficient $\propto \delta^2/\Delta t$ as $\Delta t \to 0$.

We conclude from the results of this section that if quadrature is used, then uniformly setting $\varepsilon = 0$ in Eq.(12) is good choice: It gives a stable scheme whose numerical dissipation tends to zero as Δt tends to zero. In practical terms, this implies that one uniformly distributes the ephemeral particles at the new timelevel, and computes where they came from.

4. Linear Dispersion.

The linear dispersion relation for the EPIC scheme is given by the Fourier-Laplace transform of Eq.(13) with ξ = constant:-

$$e^{i\omega\Delta t} = \tilde{S}(k,\xi)/\tilde{S}(k,0) \qquad (17)$$

where

$$\tilde{S}(k,\xi) = \sum_p S(\xi+p)\, e^{-ikp} \qquad (18)$$

We restrict our attention here to those cases where the same set of quadrature points are used to evaluate both sides of Eq.(13).

4.1 One point per element.

If we take one quadrature point per element, located at the nodes ($\delta = 1$, $\varepsilon = 0$) then

$$S(x) = \begin{cases} 1 - |x| & |x| \leq 1 \\ 0 & \text{otherwise} \end{cases}$$

and for $0 \leq \xi \leq 1$

$$\tilde{S}(k,\xi) = 1 - \xi(1 - \cos k) + i\xi \sin k \qquad (19)$$

It follows from Eq.(19) that this crude quadrature is equivalent to lumping the l.h.s. of Eq.(2). If this quadrature were only applied to the l.h.s. of Eq.(2), we find the dispersion relation

$$e^{i\omega\Delta t} = \frac{\tilde{S}(k,\xi)}{\tilde{I}(k,0)} = \frac{1-\xi(1-\cos k) + i\xi\sin k}{1 - 2/3 \sin^2 k/2}$$

which gives $|e^{i\omega\Delta t}|^2 \geq 1$ for all ξ, implying unconditional instability.

Placing the one quadrature point per element at the centre of the element ($\delta = 1$, $\varepsilon = 1/2$) gives

$$e^{i\omega\Delta t} = \frac{\tilde{S}(k,\xi)}{\tilde{S}(k,0)} = 1 + \frac{i2\xi\sin k}{1+\cos k}$$

which again is unstable since $|e^{i\omega\Delta t}| \geq 1$. As noted in the previous section, lumping or using quadrature points with offset $\varepsilon = 0$ gives stable schemes: For the case, with lumping we find

$$|e^{i\omega\Delta t}|^2 = |\tilde{S}(k,\xi)|^2 = \frac{1}{4}\left[(1+\cos k)^2 + 4\xi^2 \sin^2 k\right] \leq 1$$

4.2 Two points per element.

Taking quadrature points, $\delta = 1/2$, $\varepsilon = 1/2$ in each element gives

$\tilde{S}(k,\xi)$ piecewise linear in ξ, with minima at $\xi = 0$ and $1/2$ and maxima at $\xi = 1/4$ and $3/4$. It therefore follows from Eq.(17) that this scheme is unconditionally unstable. Lumping the mass matrix (giving dispersion relation $e^{i\omega\Delta t} = \tilde{S}(k,\xi)$) stabilises, since $\max_{(\xi,k)} |\tilde{S}(k,\xi)| = 1$. Similarly, taking quadrature points at $0, 1/2$ to evaluate the mass matrix yields scheme stable for all ξ. Both of these stabilised schemes are strongly dissipative: In the limit $\Delta t \to 0$, we find that for fixed element sizes, $\omega_i = f(k)/\Delta t$.

Taking quadrature points at 0 and 1/2 ($\delta=1/2$, $\varepsilon = 0$) gives lower dissipation unconditionally stable scheme. For this case, we find

$$S(k,\xi) = \frac{1}{4}\left[3-2\xi + (1+2\xi)\cos k + i4\xi\sin k\right] \quad 0 \leq \xi \leq 1/2$$

and hence

$$e^{i\omega\Delta t} = 1 + \xi\left[\frac{-2 + i4\cot(k/2)}{1 + 2\cot^2(k/2)}\right]$$

implying that $\left|e^{i\omega\Delta t}\right| \leq 1$, and in the limit $\Delta t \to 0$

$$\omega_i \Delta t = \xi \frac{2}{1+2\cot^2(k/2)} \qquad (20)$$

i.e. $\omega_i \to f(k)$, since $\xi \propto \Delta t$. This example is an instance of the trapezium rule applied with two points per element.

A more general $\delta = 1/2$, $\varepsilon = 0$ two point quadrature is given by the linear combination of the node centred (S_0) and element centred (S_1) one point schemes

$$S = \alpha S_0 + (1 - \alpha) S_1 \qquad (21)$$

$\alpha = 0$ and 1 recovers respectively the unstable and stable one point schemes, and $\alpha = 1/2$ gives the two point trapezium rule discussed above.

Theorem

For the set of schemes defined by Eq.(20)

i) $\alpha \geq 1/2$ gives unconditional stability

ii) the least dissipative unconditionally stable scheme has $\alpha = 1/2$, (i.e. the trapezoidal rule)

iii) the least dissipative scheme stable for Courant number $\xi \leq \xi_{max} \leq 1/2$ has $\alpha = \xi_{max}$.

Proof

By symmetry and periodicity, we need only consider the case $0 \leq \xi \leq 1/2$. In this case, we find

$$\begin{aligned} S(1-\xi) &= [1 + 2\xi + \alpha(2\xi - 1)]/4 \\ S(\xi) &= [1 - \alpha(2\xi - 1)]/2 \\ S(1+\xi) &= [1 - 2\xi + \alpha(2\xi - 1)]/4 \\ S(p+\xi) &= 0 \quad p \text{ is integer} \neq 0, \pm 1 \end{aligned}$$

Hence

$$e^{i\omega\Delta t} = \frac{\tilde{S}(k,\xi)}{\tilde{S}(k,0)} = 1 + \xi\left[\frac{-2\alpha + 2i\cot(k/2)}{\alpha + \cot^2(k/2)}\right] \qquad (22)$$

Rearranging the stability condition

$$|A|^2 = \left|\frac{\tilde{S}(k,\xi)}{\tilde{S}(k,0)}\right|^2 \leq 1$$

gives

$$\cot^2(k/2)\,(\xi - \alpha) \leq \alpha^2(1 - \xi)$$

This inequality is satisfied for all $k \in [-\pi, \pi]$ and $\xi \in [0, 1/2]$ provided $\alpha \geq 1/2$, thus establishing (i). If $\alpha < 1/2$, then the scheme is stable for Courant numbers $\xi \leq \xi_{max} = \alpha$.

In the absence of numerical dissipation $|A|^2 = 1$, and $|A|^2$ becomes smaller as dissipation increases. Damping increases with wavenumber; $\partial |A|^2 / \partial k \leq 0$ if $\alpha \leq 1$. The displacement (or Courant number) ξ_{ex} at which dissipation is maximum is

$$\xi_{ex} = \frac{\alpha(\alpha + \cot^2\theta)}{2(\alpha^2 + \cot^2\theta)}$$

and at that $\xi = \xi_{ex}$.

$$|A|^2 = \frac{1}{1 + \alpha^2 \tan^2\theta}$$

Thus, the least dissipative scheme has the smallest α compatible with stability: For unconditional stability, this is $\alpha = 1/2$, and for stability when $\xi \leq \xi_{max}$, it is $\alpha = \xi_{max}$.

Setting $\alpha = \xi$ in Eq.(22) shows that the conditionally stable scheme recovers the property of the zero quadrature error case in that $\omega_i \to 0$ as $\Delta t \to 0$.

4.3 Trapezium Rule Schemes.

Results of evaluating Eq.(17) numerically for different quadrature point spacings $\delta = 1/M$ and offsets ε are shown in figures 1-5. Plotted are the real and imaginary parts of the frequency, ω_r and ω_i, versus wavenumber k, for wavenumbers in the principal zone [4]. The differential problem (Eq.(1)) has a dispersion relation

$$\frac{\omega_r \Delta t}{\pi \xi} = \frac{k}{\pi} \quad , \quad \frac{\omega_i \Delta t}{\pi \xi} = 0$$

The deviation of the curves shown in the figures from these lines for ω_r and ω_i give measures respectively of the phase errors and numerical damping. Good numerical schemes generally have small damping for wavenumbers with small phase errors, and large damping where phase errors are large [2]. Economy of storage in multidimensional calculations favour schemes with small phase errors up to large wavenumbers, say $k = \pi/2$ (which corresponds to a wavelength of four node spacings).

Figure 1 shows the dependence of the dispersion curves on the number, M, of quadrature points per element. Figure 1a shows that once M exceeds 1, phase errors closely follow those of the integral evaluation limit ($M = \infty$). Figure 1b shows dissipation decreasing as M increases.

Figure 2 compares dissipation for different $M = 2$ cases. Curve 4 the curve is the integral limit (labelled ∞ in Fig.1). Curve 1 evaluates both sides of Eq.(12) with $\varepsilon = 1/2$, $M = 2$, confirming that this choice of quadrature is numerically unstable ($\omega_i < 0$). This may be interpreted as applying too much 'antidiffusion' by inverting the mass matrix. Curve 2 shows that using $\varepsilon = 0$, $M = 2$ on the l.h.s. and $M = 2$, $\varepsilon = 1/2$ on the r.h.s. of eq.(12) gives stable antidiffusion, but with slightly larger dissipation than obtains when $M = 2$, $\varepsilon = 0$ is used consistently (c.f. figure 1). Curve 3 is for no antidiffusion. The mass matrix on the l.h.s. of Eq.(12) is lumped to give a unit matrix, and the result, as expected, is strong numerical dissipation.

Figures 3-5 illustrate the change in dissipation with timestep. Figure 3 shows $\omega_i \to 0$ as $\Delta t \to 0$ in the absence of quadrature errors. The numbers labelling the curves are Courant numbers, ξ. Figures 4 and 5 show the same cases using $M = 4$ and $\varepsilon = 0$ for mass matrix evaluation and respectively $M = 4$, $\varepsilon = 0$ and $M = 4$, $\varepsilon = 1/2$ for evaluation of the r.h.s. Figure 4 shows $\omega_i \to$ constant as $\Delta t \to 0$ and figure 5 shows $\omega_i \to \infty$ as $\Delta t \to 0$. In all three cases, the scaling of ω_i is for fixed node spacing; If $\Delta t \to 0$ and $\Delta \to 0$, then the differential limit can be recovered. The real parts of the frequency corresponding to curves in Figs.2 - 5 differ little from those given in figure 1a.

5. Kinematic test problem.

We extend here the kinematic test problem used to compare the integral form of EPIC (Eq.(2)) with conventional finite difference schemes [1-3]. A Gaussian hump is transported through a unit length periodic box by a velocity field u(x) that provides both compression and expansion. We take $u = 2 - \sin 2\pi x$, N = 100 nodes in a spatial period and a Gaussian density hump placed initially at x = - 0.2 near the velocity maximum ($\rho(x, t = 0) = \exp[- [x + 1/5]^2/\sigma^2]$, $\sigma = 0.1$). The evolutionary equation being modelled is the continuity equation

$$\frac{\partial \rho}{\partial t} + \frac{\partial}{\partial x} (\rho u) = 0 \qquad (23)$$

We consider three approximations to Eq.(23). The integral EPIC scheme using linear trial and basis functions

$$\int W_q(x)\, \rho(x, t+\Delta t)\, dx = \int W_q(x)\, \rho(x_o, t)\, dx_o \qquad (24)$$

where $x = x_o + \xi$. The r.h.s. of Eq.(24) is a piecewise cubic, and the l.h.s. becomes a tridiagonal matrix of stencil, [1,4,1]/6 multiplying nodal values of ρ. Given ξ, each timestep comprises i) evaluating the r.h.s. of Eq.(24), and then inverting the mass matrix to obtain new nodal values, $\{\rho_p^{t+\Delta t};\ p \in (1,N)\}$.

The second case assumes uniform quadrature at the new timelevel. Setting $\chi(x) = \xi(x_o)$, we approximate Eq.(24) by

$$\sum_i W_q(x_i)\, \rho(x_i, t+\Delta t)\, \delta = \sum_i W_q(x_i)\, \rho(x_i - \chi_i, t) \frac{\partial x_o}{\partial x}\, \delta \qquad (25)$$

where $W_q(x_i)$ are 'triangle' functions [4], ρ and χ are piecewise linear, $\partial x_o / \partial x \equiv 1 - \partial\chi/\partial x$, $x_i = i\delta$, i integer and $\delta = 1/M$.

The third alternative is to use the trapezium rule on the r.h.s. of Eq.(24) at the old timelevel, and treat the l.h.s. as in Eq.(25), giving

$$\sum_i W_q(x_i)\rho(x_i,t+\Delta t)\delta = \sum_i W_q(x_{oi}+\xi(x_{oi}))\rho(x_{oi},t)\delta \qquad (26)$$

where ξ is assume linear in x_o over each element.

Figures 6 - 8 give results of the test problem. Figure 6 shows the remarkably low dispersion and numerical dissipation achieved by EPIC with integral evaluation. In the absence of numerical errors, the two curves would be identical. After the ~2000 steps in this test, the errors are smaller than are achieved by state-of-the-art finite difference schemes [2,3].

Figure 7 illustrates the effect of quadrature errors. As expected, dispersion remains small but dissipation increases as the number of quadrature points per cell is reduced.

Figures 6 and 7 are for a Courant number $\xi = 0.25$ at the position of maximum velocity. This value was chosen to afford direct comparison with results for other schemes presented in [2]. However, EPIC schemes with $\varepsilon = 0$ are unconditionally stable, so we are free to choose larger timesteps. Increasing Δt reduces the number of steps to complete the three periods, so reduces computational costs and numerical dissipation. Figure 8 illustrates this for $M = 4$, $\varepsilon = 0$ and three different Courant numbers. Note that these results are for non-uniform velocity $u(x)$. For uniform advection and integer Courant number, numerical dissipation would be zero.

6. Dynamical Test Problem.

We have applied three variations of the linear basis function EPIC scheme to Burgers' Equation

$$\frac{\partial v}{\partial t} + v\frac{\partial v}{\partial x} = R^{-1}\frac{\partial^2 v}{\partial x^2} \qquad (27)$$

on the unit period interval with initial conditions $v = -\sin 2\pi x$. The three cases are i) nonconservative, ii) conservative and iii) nonconservative with quadrature in space (ie with discrete particle

effects). In each case the diffusion term on the r.h.s. of Eq.(27) is treated fully implicitly.

Integrating the nonconservative form, Eq.(27) over a small time interval Δt gives

$$v - R^{-1} \Delta t \frac{\partial^2 v}{\partial x^2} = v_o \qquad (28)$$

where $v = v(x,t+\Delta t)$, $v_o = v(x_o,t)$, $x = x_o + \xi$ and $\xi = v_o \Delta t$. The EPIC projection equation for Eq.(28) is

$$\{\int (W_k W_l + R^{-1} \Delta t \frac{\partial W_k}{\partial x} \frac{\partial W_l}{\partial x}) \, dx\} v_l = \int W_k(x) v_o \, dx \qquad (29)$$

where $v(x) = \sum_I W_l(x) v_l$, etc.

The algorithm for advancing v by one timestep using Eq.(29) is

a) predict $x = x_o + \xi$

b) find $M_k = \int W_k(x) v_o \, dx$

c) solve $Av = M$

If required, a correction for ξ could be applied, although we find the simple prediction $\xi = v_o \Delta t$ is sufficient. Elements of matrix A are given by evaluating the integral on the l.h.s. of Eq.(29). A is tridiagonal with stencil

$$\frac{1}{6} [1 - \alpha, \; 4 + 2\alpha, \; 1 - \alpha] \; ; \quad \alpha = 6R^{-1} \Delta t$$

The conservative EPIC scheme is obtained by writing $v \partial v/\partial x$ as $\partial/\partial x(v^2/2)$ and following the above discretisation steps. In this instance

$$\xi = v_o \Delta t/2$$

and

$$\{\int(W_k W_l + R^{-1}\Delta t \frac{\partial W_k}{\partial x}\frac{\partial W_l}{\partial x})dx\} v_l = \int W_x(x) v_o dx_o \qquad (30)$$

Case iii) differs from case i) in that integrals in Eq.(29) are replaced by sums with $\varepsilon = 0$ (cf Eq.(12)). The discretisation may be interpreted as using particles which are uniformly distributed at the new timelevel.

Case i) and ii) give almost identical results. For large Reynolds number, R, the sinusoid rapidly becomes a "sawtooth', then decays on the resistive timescale. Figure 9 shows results for case i). At R = 100, v are accurately resolved and smooth. At higher R wiggles develop, but unlike many finite difference schemes, which are nonlinearly unstable at such R due to aliasing errors [6,7,8], EPIC remains stable. Finite time singularities are not possible in the limit $\Delta t \to 0$ for the EPIC schemes discussed here, since in that limit it follows from the projection equation that $d/dt \int v^2 dx < 0$. The appearance of wiggles is the Gibbs phenomenon, caused by insufficient resolution. Appropriate sub-grid-scale physics models can be used with EPIC (as with other schemes) to remove these wiggles.

The extra dissipation (cf.Fig.1) in case iii) suppresses some of the wiggles. More interestingly, the robustness of the particle advection allows much larger timesteps to be used. Figure 10 shows the solution for the test problem remains accurate as well as stable for Courant numbers up to four !

7. Final Remarks.

The Ephemeral Particle-in-Cell(EPIC) method gives stable, low dissipation and dispersion schemes for integrating the hyperbolic and nearly hyperbolic equations arising, for example, in fluid and mhd simulations. This paper has addressed the question of stability and accuracy of EPIC algorithms. The discussion has been presented in one spatial dimension but the results apply equally well in two and three dimensions.

In Section 2, the stability of EPIC algorithms for any choice of basis/trial function W was established in the integral limit. Quadrature (which may be interpreted as discrete particle effects) can in certain circumstances destroy the stability. However, in section 3 it was shown that unconditionally stable schemes can be constructed for any W and number of particles (quadrature points) per element.

Specific cases considered in Section 4 identify the unstable cases as those with too much antidiffusion. The least diffusive schemes with uniformly placed particles are those where at least one particle per element coincided with the element nodes. The kinematic and dynamic test problems confirm this, and show that choosing particle positions uniform at the new timelevel is the most effective option.

Unconditional stability allows much larger timesteps for kinematic equations than is possible with conventional finite differencing in time. One surprising feature of the dynamical test problem was that it also also remained stable. Whether this is generally true or is a special property of the test cases has not yet been established.

REFERENCES

[1] J.W.Eastwood, Particle Methods in : Astrophysical Radiation Hydrodynamics eds. K-H. A Winkler and M.L.Norman (Reidel, Holland, 1986).

[2] J.W.Eastwood and W.Arter, in : Numerical Methods for Fluid Dynamics II eds. K.W.Morton and M.J.Baines (OUP, Oxford, 1986), p.581.

[3] J.W.Eastwood, Particle Simulation Methods in Plasma Physics, Computer Phys. Commun. 43 (1986) 89.

[4] R.W.Hockney and J.W.Eastwood, Computer Simulation using Particles (McGraw-Hill, New York, 1981).

[5] P.J.Roache, Computational Fluid Dynamics, (Hermosa, Albuquerque, 1976) p.242.

[6] J.W.Eastwood and W.Arter, Phys. Rev. Lett. 57 (1986) 2528.

[7] W.Arter and J.W.Eastwood, "The Effect of Aliasing Error upon Numerical Solutions of the Hydrodynamic and Magnetohydrodynamic Equations", to appear Transp. Th.Stat. Phys. (1986).

[8] J.W.Eastwood and W.Arter, Culham Preprint CLM-P-782(1986) to appear IMA J.Numer.Anal.

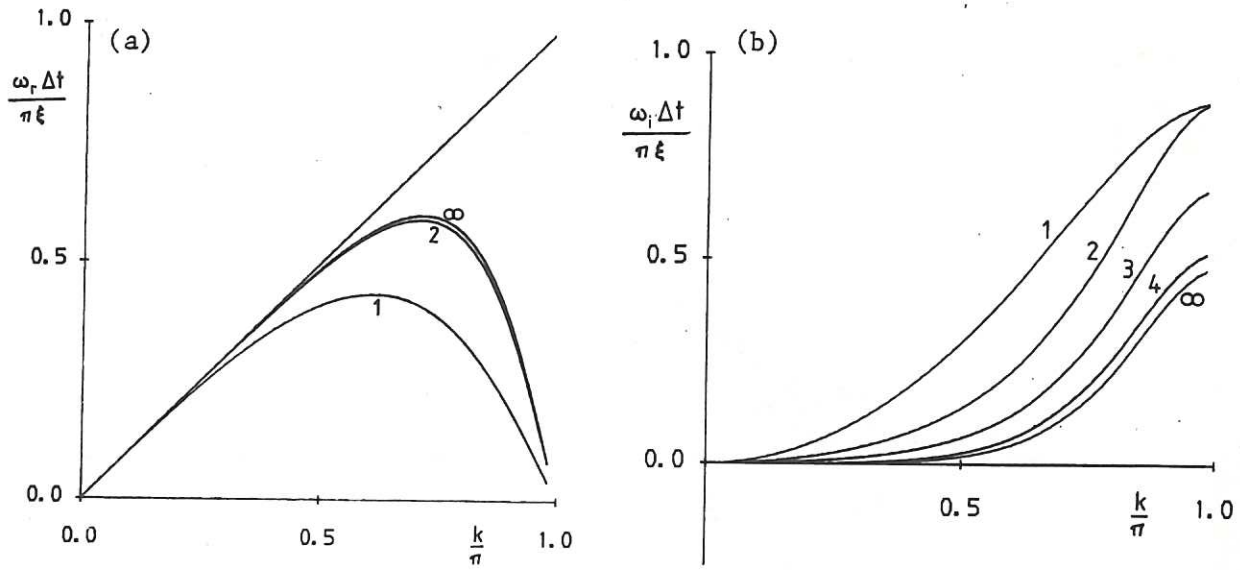

Fig. 1 Dispersion curves, a) real part and b) imaginary part of frequency versus wavenumber for the linear basis function EPIC scheme using trapezium rule integration with $\epsilon = 0$. Numbers labelling curves are values of M. Wavenumber $k = \pi$ corresponds to a wavelength of two elements. The curve labelled ∞ is the integral case.

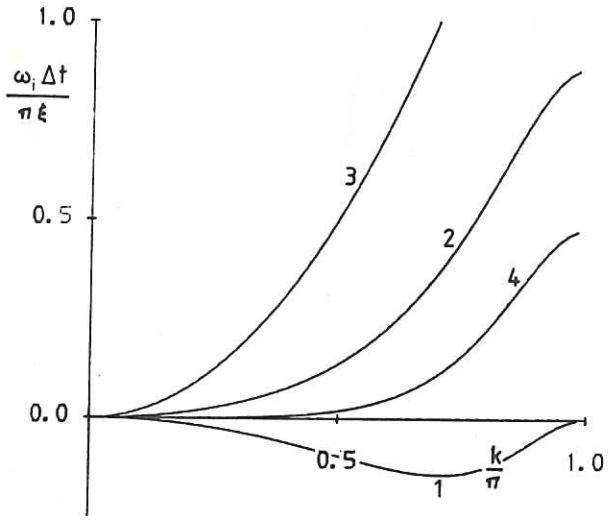

Fig. 2 Numerical dissipation for $M=2$, $\epsilon=1/2$ evaluation of assignment (r.h.s. of Eq. (12)) and evaluation of mass matrix (l.h.s. of Eq. (12)) 1) with $M=2$, $\epsilon=1/2$ 2) with $M=2$, $\epsilon=0$ and 3) lumped. Curve 4 is the integral case.

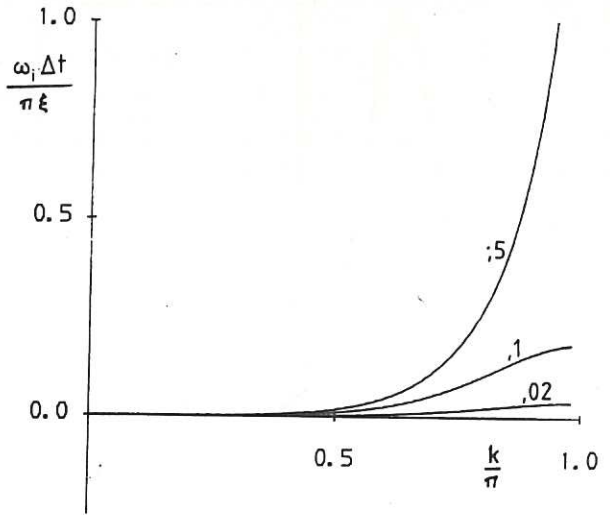

Fig. 3 Scaling of numerical dissipation with Δt for linear EPIC using exact integration (Eq.(2)), showing $\omega_i \to 0$ as $\Delta t \to 0$. The number labelling curves are Courant number, ξ.

CLM-P789

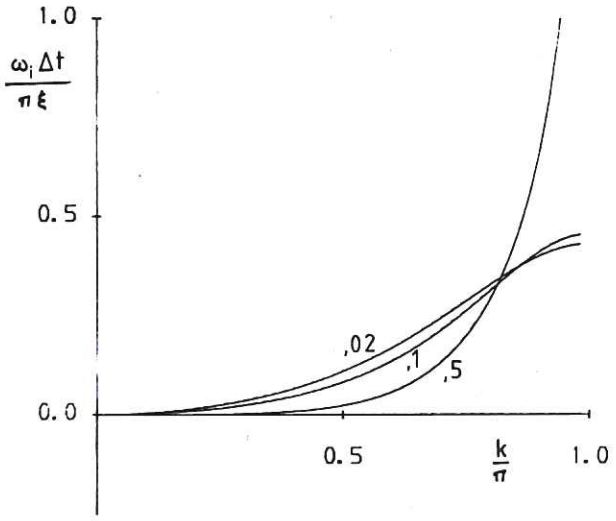

Fig. 4 Scaling of numerical dissipation for linear EPIC using trapezium rule integration with $\epsilon=0$, $M=4$, showing $\omega_i \rightarrow$ constant as $\Delta t \rightarrow 0$.

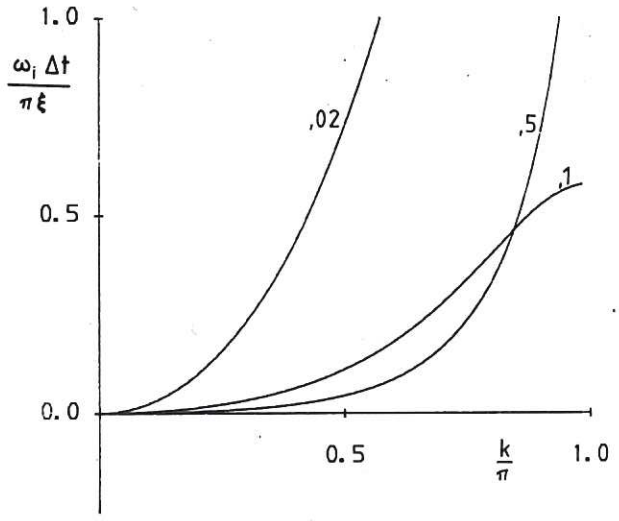

Fig. 5 Scaling of dissipation with Δt, showing ω_i increasing as Δt decreases if different quadrature is used on each side of Eq.(12) [$M=4$, $\epsilon=0$ on 1.h.s, $M=4$, $\epsilon=1/2$ on r.h.s.].

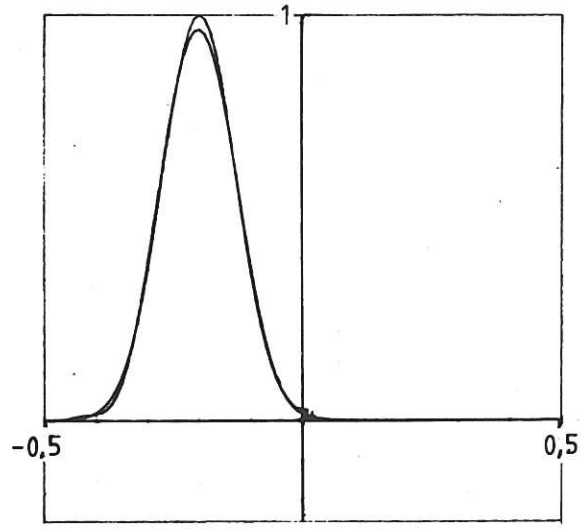

Fig. 6 Initial and final profiles of a Gaussian convected three times round a unit period by a sinusoidal velocity profile using the integral linear basis function EPIC scheme, Eq.(2). A Courant number of 0.25 was used.

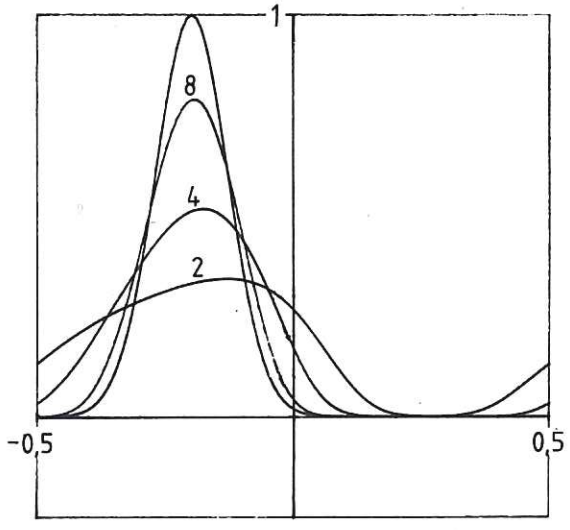

Fig. 7 As figure 6, but using uniform quadrature at the new timelevel, with $\epsilon=0$ and M as labelling the curves.

CLM-P789

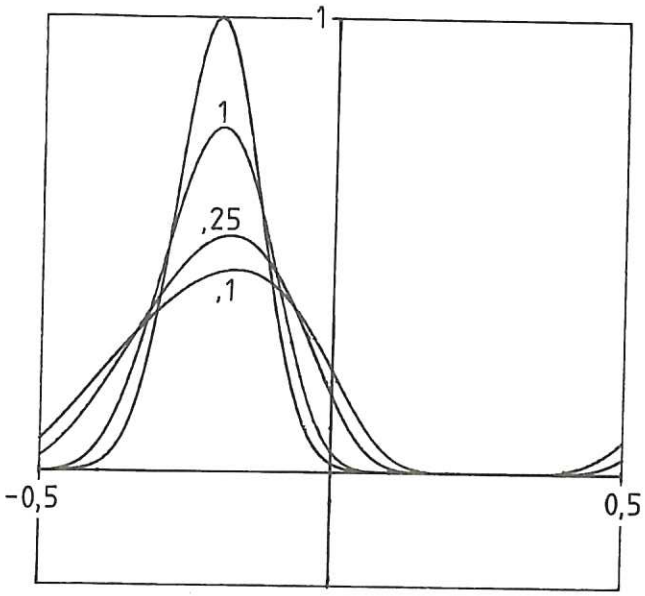

Fig. 8 The same problem as fig 7, but with $\epsilon=0$, $M=4$ and Courant numbers as labelling the curves.

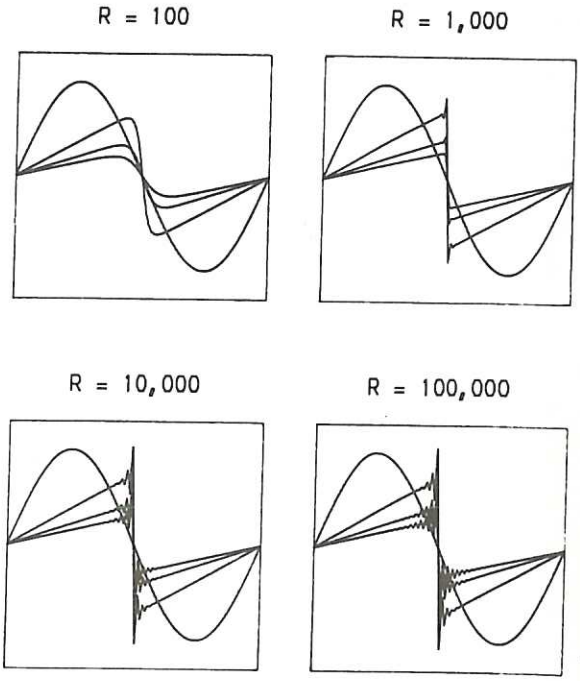

Fig. 9 Sequences showing reduction in amplitude as time increases of solutions to Burgers' Equation. Courant number=0.5, N=100 nodes and output every $100\Delta t$ were used. Reynolds numbers, R, are as indicated.

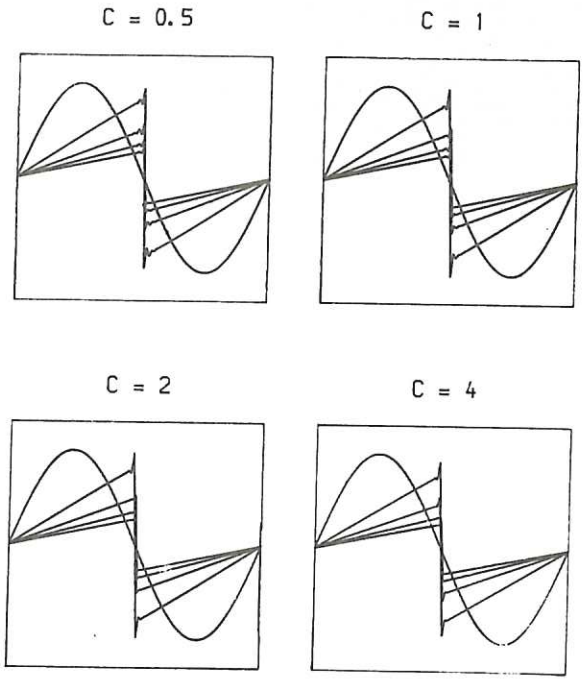

Fig. 10 Sequence showing evolution of solutions to Burgers' Equaiton using case iii) of Sec. 6, with $M=4$ particle per element predictor $\chi=v\Delta t$, $R=10^4$, N=100 and Courant numbers as shown. Curves are drawn at intervals of $40/C\Delta t$.